

Advanced light-shift compensation protocol in a continuous-wave microcell atomic clock

M. Abdel Hafiz¹, R. Vicarini¹, N. Passilly¹, C. E. Calosso², V. Maurice¹,
J. W. Pollock^{3,4}, A. V. Taichenachev^{5,6}, V. I. Yudin^{5,6,7}, J. Kitching³ and R. Boudot¹

¹*FEMTO-ST, CNRS, UBFC, ENSMM, 26 rue de l'épitahe 25030 Besançon, France*

²*INRIM, Strada delle Cacce 91, Torino, Italy*

³*National Institute of Standards and Technology, Boulder, Colorado 80305, USA*

⁴*University of Colorado, Boulder, Colorado 80309-0440, USA*

⁵*Novosibirsk State University, ul. Pirogova 1, Novosibirsk 630090, Russia*

⁶*Institute of Laser Physics SB RAS, pr. Akademika Lavrent'eva 15B, Novosibirsk 630090, Russia and*

⁷*Novosibirsk State Technical University, pr. Karla Marksa 20, Novosibirsk 630073, Russia*

(Dated: May 12, 2020)

Light-shifts are known to be an important limitation to the mid- and long-term fractional frequency stability of different types of atomic clocks. In this article, we demonstrate the experimental implementation of an advanced anti-light shift interrogation protocol onto a continuous-wave (CW) microcell atomic clock based on coherent population trapping (CPT). The method, inspired by the Auto-Balanced Ramsey (ABR) spectroscopy technique demonstrated in pulsed atomic clocks, consists in the extraction of atomic-based information from two successive light-shifted clock frequencies obtained at two different laser power values. Two error signals, computed from the linear combination of signals acquired along a symmetric sequence, are managed in a dual-loop configuration to generate a clock frequency free from light-shift. Using this method, the sensitivity of the clock frequency to both laser power and microwave power variations can be reduced by more than an order of magnitude compared to normal operation. In the present experiment, the consideration of the non-linear light-shift dependence allowed to enhance light-shift mitigation. The implemented technique allows a clear improvement of the clock Allan deviation for time scales higher than 1000 s. This method could be applied in various kinds of atomic clocks such as CPT-based atomic clocks, double-resonance Rb clocks, or cell-stabilized lasers.

I. INTRODUCTION

Atomic clocks have experienced over the last decades a remarkable evolution and progress. On the one hand, outstanding progress in laser science and technology, making possible manipulation, cooling, trapping, and probing of ultra-narrow atomic transitions, has led to the demonstration of optical atomic frequency standards with fractional frequency stability in the range of a few 10^{-17} $\tau^{-1/2}$ and accuracy approaching the 10^{-19} level [1, 2]. These instruments are exquisite tools to perform fundamental physics tests including geodesy [3, 4], Lorentz symmetry testing [5], and dark matter searching [6]. On the other hand, the combination of atomic spectroscopy, integrated photonics, and microelectromechanical systems (MEMS) has permitted the demonstration of low-power fully-miniaturized atomic clocks with stability levels below the 10^{-11} level at 1 day averaging time [7–10], finding applications in many civil and industrial systems.

For a wide variety of atomic clocks, including optical clocks based on quadrupole [11], octupole [12] and two-photon transitions [13–16], microwave vapor cell clocks based on coherent population trapping (CPT) [17–21] or optical-microwave double-resonance technique [22], light-induced frequency shifts are known to be a relevant contribution to the clock mid- and long-term frequency stability performance.

A common approach to mitigate light-shifts is to probe

the atomic resonance in pulsed operation using Ramsey spectroscopy [23]. However, with Ramsey spectroscopy, interrogation pulses themselves are responsible for non-negligible light-shifts. Thus, advanced Ramsey interrogation protocols have been proposed and demonstrated that rely on the generation of two consecutive Ramsey sequences with different dark periods and the subsequent extraction of error signal(s) for the local oscillator (LO) frequency stabilization and light-shift compensation [24–31]. Nevertheless, these methods are dedicated to pulsed-operation clocks and are not adapted for continuous-wave (CW) clocks that yet, still represent the privileged operation mode in numerous atomic clocks, including Rb cell clocks, chip-scale atomic clocks, or cell-stabilized lasers. Therefore, the establishment of light-shift suppression techniques in CW clocks is of significant interest. In two-photon optical clocks, original techniques based on the use of two interrogating laser fields at different frequencies [13], the proper tuning of a magic light-field polarization [33] or the use of a dual-color magic wavelength trap [34] have been reported. In optically-pumped Rb clocks, a method of suppressing the light-shift by adjusting the laser frequency used for optical pumping was proposed in [35]. In CPT atomic clocks, several approaches for light-shift mitigation have been proposed, including the fine tuning of the VCSEL microwave modulation index [36, 37], the compensation for the laser frequency detuning [38], the adjustment of the cell temperature to a specific setpoint [39] or solutions combining actions on both the VCSEL dc-bias current drift and on the modu-

lation index of the VCSEL light field [40]. Nevertheless, the latter techniques rely on experimentally-determined quantities that are expected to change with time and from one device to another.

In a recent study, novel universal concepts have been proposed for compensating the light-shift and its fluctuations in CW-atomic clocks [41]. In one of the proposed methods, named CW-Auto Compensated Shift (CW-ACS), the LO frequency is successively adjusted at two light-shifted frequencies obtained at two distinct laser powers through a control parameter. Assuming linearity of the light-shift, the latter is then used as an artificial anti-light shift to compensate for the actual undesired light-shift. However, to our knowledge, these techniques have never been demonstrated experimentally.

In this article, we demonstrate the experimental implementation of the CW-ACS interrogation protocol applied to a CPT-based microcell atomic clock. Inspired by [29], the CW-ACS sequence is symmetrized (CW-SACS) for cancellation at the first order of an atomic memory effect and to compensate for errors in the atomic frequency estimation induced by imperfections of the laser power modulation pattern. Original error signals are processed such that all pulses are used both for the LO frequency and light-shift correction servo loops, preventing the presence of a dead time and the loss of information. Moreover, in the reported CPT clock, an extended version of the CW-SACS technique was applied to overcome the non-linear response of the light-shift curve and then improve the light-shift reduction. Using this approach, the sensitivity of the clock frequency to laser and microwave power variations is further reduced by more than a factor 10. The implemented technique allows a clear improvement of the clock Allan deviation for time scales higher than 1000 s.

II. BASICS OF THE CW-ACS METHOD

In the present manuscript, we consider for illustration a Cs atomic system, with unperturbed clock transition frequency ν_{Cs} , that can be affected by different kinds of frequency shifts. The CW-ACS method, proposed in [41], is an attractive approach in atomic systems where light-induced frequency shifts are dominant. The main objective of the CW-ACS method is to generate a clock frequency equal to the light-shift-free frequency ν_{at} .

Let's consider first an ideal light-shift free passive atomic clock. From an experimental point of view, the LO frequency is first swept in order to detect the atomic resonance signal, characterized by its linewidth $\Delta\nu$. Hence, a dispersive error signal S , crossing zero at the resonance extremum, is obtained by probing, with $\pm\Delta\nu/2$ frequency-jumps of the LO, the signal on both sides of the atomic resonance. An iterative algorithm servo loop is then implemented to null the error signal S and then stabilize the LO frequency ν_{LO} onto the light-shift free atomic resonance ν_{at} such that $S(\nu_{LO}) \simeq -D_e(\nu_{LO} -$

$\nu_{at}) = 0$, with D_e the absolute value of the slope of the error signal S , at low detunings.

Under interaction with a light field, atoms experience a light-shift Δ_P . The zero-crossing of the error signal is therefore shifted by Δ_P , leading the LO frequency to be stabilized onto a light-shifted frequency, since the servo loop operates to satisfy $S(\nu_{LO}) \simeq -D_e(\nu_{LO} - (\nu_{at} + \Delta_P)) = 0$. Moreover, since this signal depends on the laser power, laser power variations will induce frequency instabilities. Let's consider now two light-shifted error signals S_1 and S_2 obtained at two laser powers P_1 and P_2 , such that $P_2 > P_1$. Linearity of the light-shift is assumed such that the actual light-shift at the power P_1 (P_2) is $\Delta_{P_1} = cP_1$ ($\Delta_{P_2} = cP_2$), with c the coefficient of proportionality. The essence of the CW-ACS method is then for any laser power P to shift the frequency sent to the atoms ν_{LO} from the unperturbed resonance frequency by an amount ξP so that $\nu_{LO} = \nu_0 + \xi P$, where ν_0 and ξ are two variable control parameters that, respectively, estimate the light-shift free frequency ν_{at} and the actual light-shift cP , such that $\xi P - cP = 0$. In an operation sequence where the laser power is alternated between two values P_1 and P_2 , the output result is equivalent to a system of two equations with two unknown variables ν_0 and ξ such that the two error signals are:

$$S_1(\nu_0 + \xi P_1) = -D_{e_1} (\nu_0 + \xi P_1 - \nu_{at} - cP_1) = 0 \quad (1)$$

$$S_2(\nu_0 + \xi P_2) = -D_{e_2} (\nu_0 + \xi P_2 - \nu_{at} - cP_2) = 0 \quad (2)$$

with D_{e_i} the slope of the error signal at the power P_i , with $i = 1, 2$. Solutions to this system are given by the relations:

$$\nu_0 = \nu_{at} \quad (3)$$

$$\xi = c \quad (4)$$

establishing that the CW-ACS method permits stabilization of the frequency ν_0 onto the light-shift free atomic frequency ν_{at} and to determine the amount of actual light shifts $\Delta_{P_1} = cP_1$ and $\Delta_{P_2} = cP_2$.

III. SYMMETRIC CW-ACS SEQUENCE

Figure 1 illustrates the CW-SACS interrogation sequence we applied to a CPT-based microcell atomic clock, where $A\nu_i P_i$, with $i = 1, 2$, denotes the averaged atomic signal over a step with LO frequency ν_i and laser power P_i . This sequence is divided into two CW-ACS sub-sequences. In each sub-sequence, the laser power is successively tuned at values P_1 and P_2 , such that $P_2 > P_1$. In the first sub-sequence, the CPT signal detection is performed by tuning first the LO frequency ν_{LO} at $\nu_0 + \xi P_1 \mp \Delta\nu_1/2$ (the left then the right side of the resonance) with light power P_1 , and then at $\nu_0 + \xi P_2 \mp \Delta\nu_2/2$ with power P_2 . The applied modulation depths equal the CPT resonance linewidth $\Delta\nu_1$ ($\Delta\nu_2$) measured at the power P_1 (P_2). In the second sub-sequence, the detection is performed by tuning first the LO frequency at

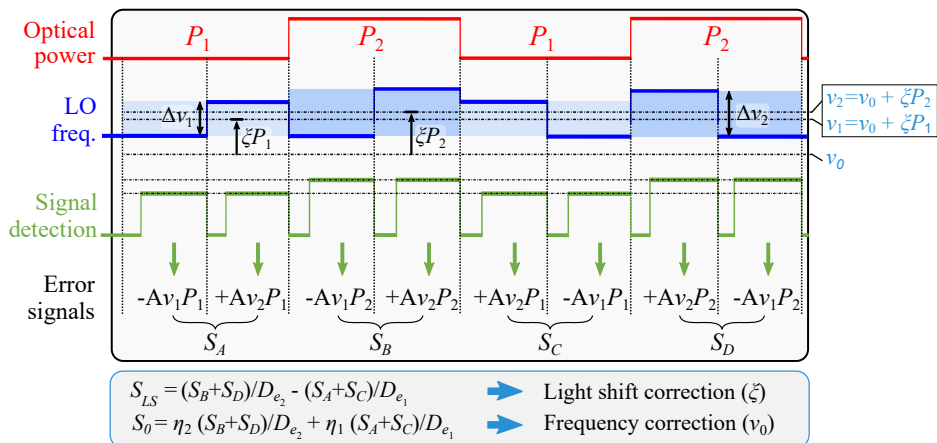


FIG. 1. Symmetric CW-ACS sequence applied to a microcell CPT-based atomic clock. Av_iP_i , with $i = 1, 2$, denote the respective atomic signal values acquired at half-height of the resonance along the sequence. Sign (+ or -) attached to the signal values Av_iP_i are those considered to calculate the error signals S_A to S_D . In our experiment, the LO modulation frequency is 1.45 kHz. The photodiode signal is acquired (signal detection) after a delay of 70 μs at each probe frequency change. This delay corresponds roughly to the response time of the laser frequency servo.

$\nu_0 + \xi P_1 \pm \Delta\nu_1/2$ (at the right then the left side of the resonance) with light power P_1 , then at $\nu_0 + \xi P_2 \pm \Delta\nu_2/2$ with power P_2 .

In the first (second) sub-sequence, two successive error signals S_A and S_B (S_C and S_D) are extracted for power values P_1 and P_2 , respectively. In comparison with the CW-ACS proposal reported in [41], an important difference is the use of an extended symmetric sequence. The CW-ACS sequence is symmetrized first to cancel at the first order a memory effect of the atoms. This memory effect, already highlighted in the case of a pulsed Ramsey-CPT clock [29], is explained here from a qualitative point of view. The key point is to understand that the atomic signal detected at a given time t , instead of depending only on the actual probing frequency at this time t , carries also, for a period equivalent to the population and CPT coherence relaxation times [42], some information related to preceding levels of the interrogation microwave and laser fields. In the present experiment, the population of atoms in the CPT state is higher at P_2 than at P_1 and it takes for this population up to a few milliseconds to stabilize after a change in the laser power set point. This results in a deviation of the atomic signal from the one obtained when no power modulation is applied. The deviation is enforced (reduced) if, during the previous step, the microwave frequency is on the same (opposite) side of the atomic resonance with respect to the current one. Considering the first half of the total symmetric sequence shown in Fig. 1, one expects then Av_1P_1 to be slightly positively offset and Av_1P_2 negatively offset. The value of the detected atomic signal S_A is then overestimated and the value of S_B underestimated. This error is then compensated at the first order with the second half of the sequence shown in Fig. 1 during which the LO frequency modulation pattern is the mirror symmetric to the one used in the first half of the sequence. The second re-

ason to use a symmetric sequence is that the laser power modulation pattern, generated in this manuscript using an acousto-optic modulator (AOM), exhibits experimentally slight transient-type imperfections. The atomic signal detected at the output of the cell is then polluted by spurious voltage offsets that induce frequency offsets in the estimation of the atomic resonant frequency.

Successive error signals (S_A to S_D) acquired along the sequence are combined to produce two output error signals. The first output error signal S_{LS} , such that:

$$S_{LS} = \frac{S_B + S_D}{D_{e_2}} - \frac{S_A + S_C}{D_{e_1}} \simeq -2(\xi - c)(P_2 - P_1) \quad (5)$$

is equivalent to a weighted difference of (1) and (2) and is representative of the residual light-shift. It is nulled by an integrative controller that corrects the control parameter ξ , in order to compensate for the light-induced frequency shift. Once the light-shift is compensated, a second output error signal S_0 , defined by;

$$S_0 = \eta_2 \frac{S_B + S_D}{D_{e_2}} + \eta_1 \frac{S_A + S_C}{D_{e_1}} \simeq -2(\nu_0 - \nu_{at}) \quad (6)$$

is calculated and is used by a second integrative controller for correcting the base frequency ν_0 , so that it converges to the light-shift free frequency ν_{at} . η_1 and η_2 are two weighting coefficients ($\eta_1 + \eta_2 = 1$) that can be used to improve the short-term stability if they are inversely proportional to the short-term stability of the clock at powers P_1 and P_2 , respectively [43].

The use of the combination of Eqs (5) and (6) is advantageous for two main reasons. The first reason is that all error signals (S_A, S_B, S_C, S_D) are used in both servo loops, preventing the presence of a dead time and the consequent loss of information through aliasing [44]. In this way, the noise in the estimations is reduced, with

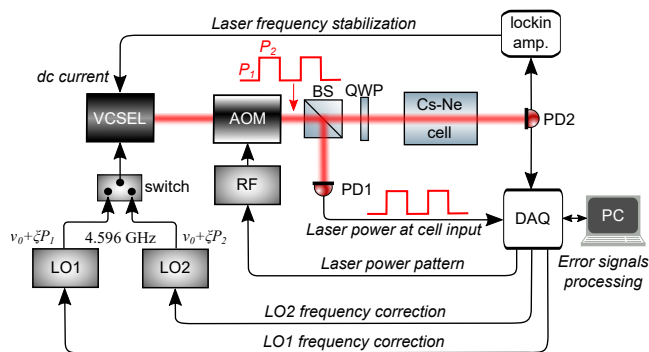


FIG. 2. CPT clock experimental setup for test of the CW-SACS method.

beneficial effects on the short-term stability of the clock. The latter, is further optimized by the weighting coefficients η_1 and η_2 , which allow to combine optimally the short-term stability of the clock at different laser powers, in case they are different. The second reason is that S_0 is a direct representative of the difference $\nu_0 - \nu_{at}$ in closed-loop operation, while S_{LS} carries directly the residual light-shift information, in any condition and independently of ν_0 . This configuration shows high decoupling of the two loops and prevents them to interfere with each other. It is interesting to note that the normalization through D_{e_1} and D_{e_2} and weighting do not change the solution of Eqs (1) and (2) and the knowledge of their exact value is not critical like in other methods such as in the CW-CES method presented in [41]. Nevertheless, their use is important from an experimental point of view, since (5) and (6) allow to consider and optimize noise and robustness, whereas these aspects are not usually taken into account by this kind of methods.

IV. EXPERIMENTAL SET-UP

The symmetric CW-ACS sequence was tested in the CPT-based microcell atomic clock described in Fig. 2. The laser source is a vertical-cavity surface emitting laser (VCSEL) tuned on the Cs D_1 line at 894.6 nm [45]. The injection current of the VCSEL is directly microwave-modulated at 4.596 GHz in order to produce two first-order optical sidebands separated by 9.192 GHz for the CPT interaction. An AOM, driven by a radiofrequency (RF) synthesizer, is used to produce laser power modulation and generate consecutive laser powers P_1 and P_2 . At the output of the AOM, a fraction of the laser power is reflected by a beam splitter and detected by a photodiode (PD1) before the cell input. The transmitted laser beam is circularly polarized using a quarter-wave plate (QWP) to produce the CPT interaction in the vapor cell. The heart of the atomic clock is a Cs microfabricated cell [46], filled with a Ne buffer gas pressure of about 93 Torr [47]. The CPT interaction takes place in a cavity of the cell with a diameter of 2 mm and a length of 1.4 mm.

The cell is temperature-stabilized at about 82°C for reduced sensitivity of the clock frequency to cell temperature variations [48, 49]. A static quantization magnetic field is produced in order to raise the Zeeman degeneracy and isolate the 0-0-clock transition. A mu-metal shield is used to protect the cell from external magnetic field perturbations. The laser power transmitted through the cell is detected by a photodiode (PD2) from which the atomic signal information is extracted. In the first path, this signal is used with the help of a lock-in amplifier for laser frequency stabilization onto the bottom of the absorption profile ($F'=4$ excited state). In the second path, the signal is acquired by a I/O multi-function card. The latter manages the CW-SACS sequence generation as well as the extraction of the error signals for frequency stabilization of the clock on the light-shift free frequency. In the paper proposing the CW-ACS method [41], the use of an additional electronic block (frequency shifter) able to shift the LO frequency for any laser power by the correct light-shift value was suggested. In our setup, the real-time management with a single LO block of the CW-SACS sequence was challenging due to the limited performance of our multi-function card. Thus, we chose for demonstration to alternately drive the VCSEL with two commercial frequency synthesizers, referenced by the same source, using a high-isolation (55 dB at 4.6 GHz) broadband switch as a microwave multiplexer. The first (second) synthesizer generates the shifted frequency $\nu_1 = \nu_0 + \xi P_1$ ($\nu_2 = \nu_0 + \xi P_2$) and associated frequency jumps $\pm\Delta\nu_1/2$ ($\pm\Delta\nu_2/2$) to probe the CPT resonance at the power P_1 (P_2). Frequency values of both LO synthesizers are then kept resonant with the light-shifted atomic frequencies, in agreement with their respective individual power values. The light-shift free atomic frequency ν_0 is then simply computed from frequencies ν_1 and ν_2 . Note that for simplicity of experiments, we chose to apply frequency-jumps $\Delta\nu_1 = \Delta\nu_2 = 2.5$ kHz, whatever the laser power. The servo gains were adapted to have roughly the same servo bandwidth for all experiments.

V. EXPERIMENTAL RESULTS

Figure 3 shows two CPT resonances and their associated error signals S_1 and S_2 obtained at respective power values $P_1 = 27.4 \mu\text{W}$ and $P_2 = 59.7 \mu\text{W}$, for a microwave power P_μ of 4.17 dBm. At the power value P_1 (P_2), the CPT resonance linewidth is 4.4 (6.5) kHz and the CPT resonance contrast is 1.2 % (3.9 %). The slope of the CPT error signal is in absolute value 3.0 and $6.8 \mu\text{V}/\text{Hz}$, for power values P_1 and P_2 respectively. For both powers P_i , with $i = 1, 2$, the totally shifted clock frequency, identified by the zero-crossing of the error signal, is $\nu_{Cs} + \Delta_Z + \Delta_{bg} + \Delta_{P_i} = \nu_{at} + cP_i$, where Δ_Z and Δ_{bg} , both independent of the laser power, are respectively the Zeeman shift (~ 4.27 Hz) and the buffer gas-induced collisional frequency shift [49], and $\Delta_{P_i} = cP_i$ is the light-shift. From Fig. 3, we find a light-shift ratio $\Delta_{P_2}/\Delta_{P_1}$

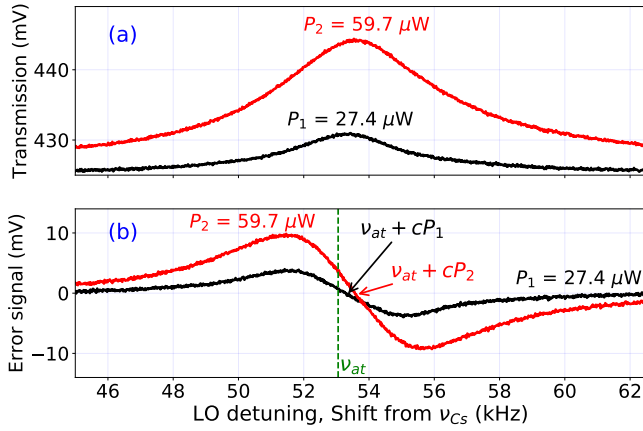


FIG. 3. (Color online) CPT resonances (a) and associated error signals (b) obtained at two different laser powers $P_1 = 27.4 \mu\text{W}$ and $P_2 = 59.7 \mu\text{W}$. An offset of 0.51 V was subtracted from the CPT resonance measured at P_2 for clarity. The green vertical dashed line shows the approximate position of the light-shift free frequency ν_{at} . Light-shifted frequencies $\nu_{at} + cP_1$ and $\nu_{at} + cP_2$, identified by the zero-crossing of the error signals, are indicated by arrows.

$\sim 570 \text{ Hz}/274 \text{ Hz} \sim 2.08 \pm 0.06$ for a power ratio $P_2/P_1 \sim 2.18 \pm 0.01$. The slight discrepancy between these two ratios can be explained by the actual non-linearity of the light-shift dependence, as highlighted later in the manuscript.

Figure 4 shows a temporal plot in clock operation using the symmetric CW-ACS sequence. This test is performed with a microwave power of 2.17 dBm. During the clock run, light-shifts induced by sudden laser power jumps (vertical dashed grey lines) are applied while frequencies ν_1 , ν_2 , and ν_0 are recorded. A significant variation of both frequencies ν_1 and ν_2 is observed at each laser power change whereas the value of the frequency ν_0 is less affected by laser power variations. In this test, the total P_2 power change of $70.5 \mu\text{W}$ induces a 1060 Hz change of the frequency ν_2 , yielding a sensitivity of about $15 \text{ Hz}/\mu\text{W}$, i.e. $1.6 \times 10^{-9}/\mu\text{W}$ in fractional value. This sensitivity is similar for the frequency ν_1 , whereas it is reduced to the level of about $3 \text{ Hz}/\mu\text{W}$ for the frequency ν_0 . This result demonstrates a reduction of the light-shift coefficient (LSC) by about a factor 5 in the CW-SACS mode.

Extracted from sequences similar to the one shown in Fig. 4, Fig. 5 shows the total clock frequency shift (referenced to the unperturbed Cs frequency $\nu_{Cs} = 9.192631770 \text{ GHz}$) versus the laser power at the cell input, for different microwave powers P_μ , in the standard CW interrogation scheme (without any light-shift mitigation technique), in comparison with the symmetric CW-ACS scheme. In the standard mode, the LSC decreases with increased microwave power. It is about $22 \text{ Hz}/\mu\text{W}$ and $10 \text{ Hz}/\mu\text{W}$ for microwave powers of 0.17 dBm and 4.17 dBm, respectively. For modulation powers higher than 4.17 dBm, we found that the CPT contrast and then the clock short-term frequency stability started to

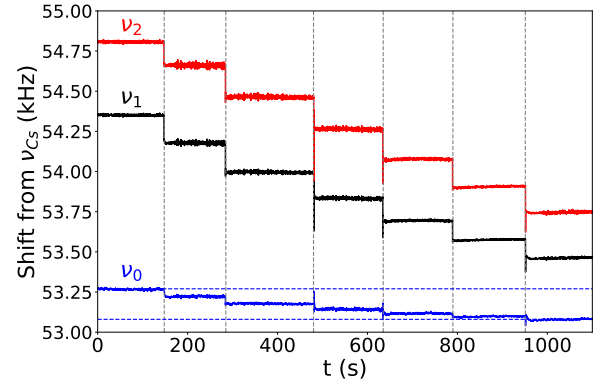


FIG. 4. Measurement of frequencies ν_1 , ν_2 , and ν_0 (frequency shift relative to ν_{Cs}) in a clock run using the symmetric CW-ACS sequence. Each power jump is shown by a vertical dashed line. For the total span, the power P_1 (P_2) is changed from 80.5 to $25 \mu\text{W}$ (114 to $43.5 \mu\text{W}$). Each power jump corresponds to a 1 dB variation on the RF synthesizer driving the AOM used to control the laser power. The microwave power P_μ is 2.17 dBm. The $\pm 2.5 \text{ kHz}$ frequency-jumps are applied for each power P_1 and P_2 to scan the CPT resonances. The power modulation depth is 35 %.

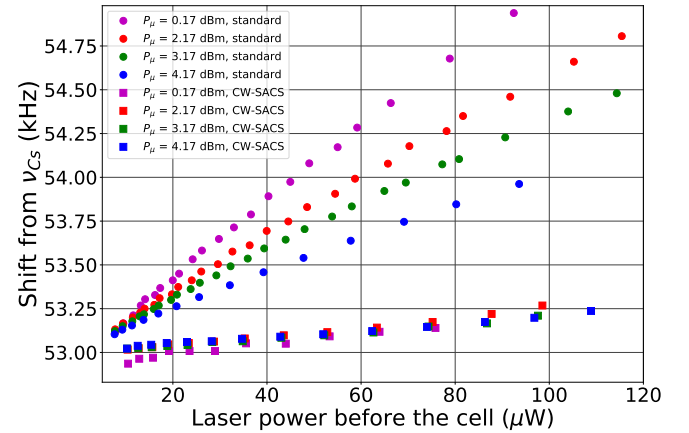


FIG. 5. Clock frequency shift (referenced to ν_{Cs}) versus the laser power at the cell input, for different microwave powers (0.17, 2.17, 3.17, and 4.17 dBm) driving the VCSEL, in standard (circles) or CW-SACS operation (squares). For the CW-SACS case, the average power $(P_1 + P_2)/2$ is considered. Error bars are smaller than the data points symbols.

degrade due to reduction of the power contained in CPT-resonant first-order sidebands. The short-term stability of the CPT clock being optimal for laser powers between $20 \mu\text{W}$ and $60 \mu\text{W}$, we focused the following analysis in this range. In the CW-SACS mode, the residual LSC in the 20 - $60 \mu\text{W}$ power range is about $2 \text{ Hz}/\mu\text{W}$, independent of the microwave power value. This sensitivity is 11 and 5 times smaller than the one obtained in the standard operation mode, at $P_\mu = 0.17 \text{ dBm}$ and 4.17 dBm , respectively. This result shows firstly that the CW-SACS method is attractive to obtain light-shift mitigation, in-

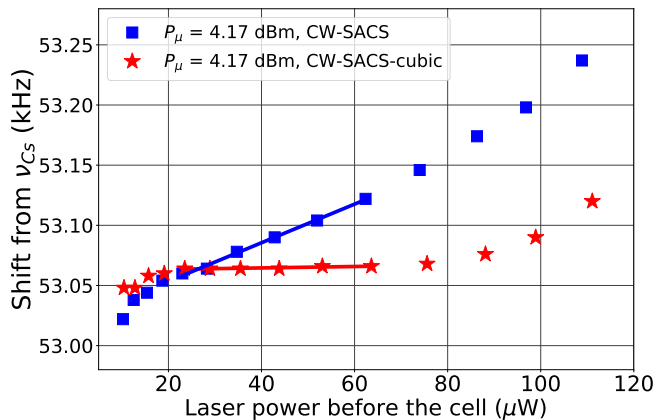


FIG. 6. Clock frequency shift (referenced to ν_{Cs}) versus the laser power at the cell input using CW-ACS with two different approximations (squares: linear; stars: cubic) for the light-shift dependence. The microwave power is $P_\mu=4.17$ dBm. Error bars are smaller than the data points symbols. Solid lines indicate a linear fit to the data points, in the 20-63 μW range.

dependently of the laser power working point. In addition, we find from Fig. 5 that the CW-SACS method reduces at fixed laser power the impact of microwave power variations on the clock frequency by about one order of magnitude.

Looking at Fig. 5, which shows light shift measurement in a wider power range, a deviation of the power light-shift curve from a linear behaviour is observed. Such a non-linear light-shift behaviour, confirmed by plotting residuals obtained from the linear fit of experimental data points (not shown here), has already been reported in CPT spectroscopy [21, 36]. The rigorous theoretical explanation of this behaviour is not treated here. However, we stress that this deviation from the ideal linear light-shift response causes two main limitations to the CW-ACS method discussed here. The first one is the presence of a finite residual light-shift sensitivity contributing to degrade the clock stability. The second one is the presence of a finite clock frequency shift from the unperturbed transition frequency which depends on the absolute values of P_1 and P_2 and on their mutual difference. Thus, it is necessary to account for the light-shift non-linearity in order to improve the light-shift mitigation efficiency.

For this purpose, we extended the CW-ACS sequence algorithm by performing in a limited power range (20-63 μW) a third-order polynomial fit of experimental data. Definitions of $\Delta_{P_1} = \xi P_1$ and $\Delta_{P_2} = \xi P_2$ were therefore changed to $\xi P_1 + \beta P_1^2 + \gamma P_1^3$ and $\xi P_2 + \beta P_2^2 + \gamma P_2^3$, at powers P_1 and P_2 , respectively. The second- (β) and third-order (γ) coefficients were extracted from the cubic fitting of experimental data and kept fixed during clock operation while ξ is continuously calculated by the light-shift servo loop.

Figure 6 displays the total clock frequency shift (from

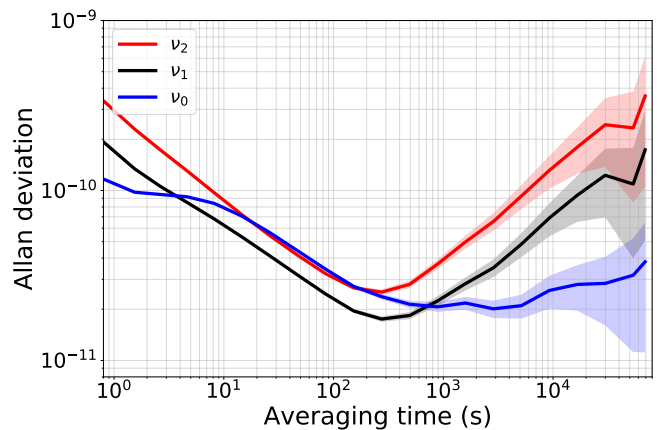


FIG. 7. Allan deviation of the frequencies ν_1 , ν_2 , and ν_0 with CW-ACS using the cubic law approximation. Data are extracted from a measurement of 58 h and 33 minutes. Error bars are illustrated by lighter-colored zones.

the Cs atom frequency ν_{Cs}) versus the cell input laser power in the CW-SACS mode, for a microwave power of 4.17 dBm, when a linear or a cubic approximation is performed. In the 20-63 μW power range, the use of the cubic approximation reduces the LSC at the level of 0.059 Hz/ μW , i.e. $6.4 \times 10^{-12}/\mu\text{W}$ in fractional value. This value is 28 times smaller than with the CW-SACS method using the linear approximation of the light-shift dependence, and a factor 170 smaller than the one obtained in standard operation in the same conditions. We insist that the cubic-law approach can be employed here since we focus on demonstrating insensitivity to light-shifts but are not concerned with clock frequency accuracy.

Finally, we have performed measurements of the clock Allan deviation in the CW-SACS mode with the cubic function approximation of the light-shift dependence. Values of ν_1 , ν_2 , and ν_0 were recorded throughout the whole sequence. The microwave power is 4.17 dBm. The clock is operated with power values $P_1 = 28.4 \mu\text{W}$ and $P_2 = 62.0 \mu\text{W}$. We used $\eta_1 = \eta_2 = 0.5$ and no specific short-term stability optimization was performed by tuning the values of these coefficients. The short-term stability of the frequency ν_1 , measured to be about $1.8 \times 10^{-10} \tau^{-1/2}$ until 200 s, is better than that of ν_2 ($3 \times 10^{-10} \tau^{-1/2}$). This is due to the fact that P_1 is closer than P_2 to the laser power (about 35 μW) that optimizes the clock short-term stability. In comparison with the standard clock configuration (single LO, no light-shift mitigation applied, laser power = 35 μW), we observed a degradation in the short-term stability by a factor of 4 for the frequency ν_1 . This degradation is partly explained by the power values choice mentioned above. In addition, sudden changes in optical power possibly degrading the laser frequency stabilization and the unusual simultaneous operation of two synthesizers might have contributed. Assuming the same fractional stability of the laser power

at P_1 and P_2 and the same clock frequency sensitivity of about $10 \text{ Hz}/\mu\text{W}$ for both power values, the medium-term stability ($\tau > 100 \text{ s}$) of ν_1 is expected to be about 0.46 times better than the stability of ν_2 , since $P_1 = 0.46 P_2$. The plot shown in Fig. 7 is in agreement with this prediction and the mid-term stability of ν_1 and ν_2 is limited by the stability of the laser power.

The short-term stability of the frequency ν_0 is similar to that of ν_2 from 10 to 200 s. The bump at 10 s is attributed to the light-shift servo loop time constant. For timescales higher than 1000 s, the stability of the light-shift free frequency ν_0 is clearly better than that of the light-shifted frequencies ν_1 and ν_2 , with a stability level remaining in the $2\text{-}3 \times 10^{-11}$ range until $6 \times 10^4 \text{ s}$. This result demonstrates further that the CW-SACS technique helps to mitigate the contribution of light-shift effects to the frequency stability of atomic clocks.

VI. CONCLUSIONS

In conclusion, we have experimentally demonstrated a technique to mitigate light-shifts in a CW-CPT-based microcell atomic clock using a symmetric CW-ACS interrogation protocol [41]. Two output error signals, constructed from the linear combination of consecutive signals acquired during the power-modulation based sequence, are used in a dual-loop system to generate a clock frequency free from light-shift. The clock frequency sensitivity to laser and microwave power variations can be reduced by one order of magnitude using the CW-SACS

sequence. Improved mitigation was achieved in our CPT clock by approximating the light-shift dependence with a third-order polynomial function in the power range of interest. Tested on a similar clock setup and similar environmental conditions, the CW-SACS technique using cubic fitting of the light-shift dependence improved the clock Allan deviation for timescales higher than 1000 s. A more accurate understanding of light-shift mechanisms with an analytical expression that fits better to experimental data will certainly help to further improve the efficiency and robustness of this method.

ACKNOWLEDGMENTS

The authors thank Azure Hansen and Joe Christensen (NIST) for careful reading of the manuscript before submission. The authors acknowledge Moshe Shuker for fruitful discussions on light-shift suppression techniques. This work was supported in part by Délégation Générale de l'Armement, in part by Région de Franche-Comté, and in part by Agence Nationale de la Recherche (ANR) in the frame of the LabeX FIRST-TF (Grant ANR 10-LABX-0048), EquipX Oscillator-IMP (Grant ANR 11-EQPX-0033) and ASTRID PULSACION (Grant ANR-19-ASTR-0013-01) projects. V. I. Yudin was supported by the Russian Foundation for Basic Research (grant 20-02-00505), the Foundation for the Advancement of Theoretical Physics and Mathematics "BASIS". This work is a contribution of NIST, an agency of the U.S. government, and is not subject to copyright.

-
- [1] M. Schioppo et al., Ultrastable optical clock with two cold-atom ensembles, *Nat. Photon.* **11**, 48 (2017).
 - [2] E. Oelker et al., Demonstration of 4.8×10^{-17} stability at 1 s for two independent optical clocks, *Nature Photonics* **13**, 714-719 (2019).
 - [3] J. Grotti et al., Geodesy and metrology with a transportable optical clock, *Nature Physics* **14**, 437 (2018).
 - [4] W. F. McGrew et al., Atomic clock performance enabling geodesy below the centimetre level, *Nature* **564**, 87-90 (2018).
 - [5] C. Sanner, N. Huntemann, R. Lange, C. Tamm, E. Peik, M. Safranov and S. G. Porsev, Optical clock comparison for Lorentz symmetry testing, *Nature* **567**, 204-208 (2019).
 - [6] P. Wcislo et al., New bounds on dark matter coupling from a global network of optical atomic clocks, *Science Advances* **4**, 12 (2018).
 - [7] R. Lutwak et al., The Chip-Scale Atomic Clock-Prototype Evaluation, *Proceedings of the 39th Annual Precise Time and Time Interval Meeting*, pp. 269-290 (2007).
 - [8] J. Kitching, Chip-scale atomic devices, *Appl. Phys. Rev.* **5**, 031302 (2018).
 - [9] H. Zhang et al. ULPAC: A Miniaturized ultralow-power atomic clock, *IEEE Journ. Solid State Circ.* **54**, 11, 3135-3148 (2019).
 - [10] R. Vicarini et al., Mitigation of temperature-induced light-shift effects in miniaturized atomic clocks, *IEEE Ultrason. Ferroelec. Freq. Contr.* **66**, 12, 1962-1967 (2019).
 - [11] Y. Huang, J. Cao, P. Liu, K. Liang, B. Ou, H. Guan, X. Huang, T. Li, and K. Gao, Hertz-level measurement of the $^{40}\text{Ca}^+4s^2S_{1/2} - 3d^2D_{5/2}$ clock transition frequency with respect to the SI second through the Global Positioning System, *Phys. Rev. A* **85**, 030503 (2012).
 - [12] K. Hosaka, S. A. Webster, A. Stannard, B. R. Walton, H. S. Margolis and P. Gill, Frequency measurement of the $^2S_{1/2} - ^2F_{7/2}$ electric octupole transition in a single $^{171}\text{Yb}^+$ ion, *Phys. Rev. A* **79**, 033403 (2009).
 - [13] V. Gerginov and K. Beloy, Two-photon optical frequency reference with active ac Stark shift cancellation, *Phys. Rev. Appl.* **10**, 014031 (2018).
 - [14] Z. L. Newman et al., Architecture for the photonic integration of an optical atomic clock, *Optica* **6**, 5, 680 (2019).
 - [15] K. W. Martin, G. Phelps, N. D. Lemke, M. S. Bigelow, B. Stuhl, M. Wojcik, M. Holt, I. Coddington, M. W. Bishop, and J. H. Burke, Compact optical atomic clock based on a two-photon transition in rubidium, *Phys. Rev. Applied* **9**, 014019 (2018).

- [16] K. W. Martin, B. Stuhl, J. Eugenio, M. S. Safronova, G. Phelps, J. H. Burke, and N. D. Lemke., Frequency shifts due to Stark effects on a rubidium two-photon transition, *Phys. Rev. A* **100**, 023417 (2018).
- [17] P. R. Hemmer, M. S. Shahriar, V. D. Natoli, and S. Ezekiel, AC Stark shifts in a two-zone Raman interaction, *J. Opt. Soc. Am. B* **6**, 1519 (1989).
- [18] Y. Yano, W. J. Gao, S. Goka, and M. Kajita, Theoretical and experimental investigation of the light shift in Ramsey coherent population trapping, *Phys. Rev. A* **90**, 013826 (2014).
- [19] M. Abdel Hafiz, G. Coget, P. Yun, S. Guérandel, E. de Clercq and R. Boudot, A high-performance Raman-Ramsey Cs vapor cell atomic clock, *J. Appl. Phys.* **121**, 104903 (2017).
- [20] P. Yun, F. Tricot, C. E. Calosso, S. Micalizio, B. Francois, R. Boudot, S. Guérandel, and E. de Clercq, High-performance coherent population trapping clock with polarization modulation, *Phys. Rev. Applied* **7**, 014018 (2017).
- [21] J. W. Pollock, V. I. Yudin, M. Shuker, M. Y. Basalaev, A. V. Taichenachev, X. Liu, J. Kitching, and E. A. Donley, ac Stark shifts of dark resonances probed with Ramsey spectroscopy, *Phys. Rev. A* **98**, 053424 (2018).
- [22] N. Almat, M. Gharavipour, W. Moreno, F. Gruet, C. Affolderbach, G. Miletì, Long-term stability analysis toward $< 10^{-14}$ level for a highly compact POP Rb cell atomic clock, *IEEE Trans. Ultrason. Ferroelec. Freq. Contr.* **67**, 1, 207-216 (2020).
- [23] N.F. Ramsey, A molecular beam resonance method with separated oscillating fields, *Phys. Rev.* **78**, 695 (1950).
- [24] C. Sanner, N. Huntemann, R. Lange, C. Tann and E. Peik, Auto-balanced Ramsey spectroscopy, *Phys. Rev. Lett.* **120**, 053602 (2018).
- [25] V. Yudin, A. V. Taichenachev, M. Yu. Basalaev, T. Zanon-Willette, J. W. Pollock, M. Shuker, E. A. Donley, and J. Kitching, Generalized autobalanced Ramsey spectroscopy of clock transitions, *Phys. Rev. Appl.* **9**, 054034 (2018).
- [26] T. Zanon-Willette, R. Lefevre, R. Metzendorff, N. Sillitoe, S. Almonacil, M. Minissale, E. de Clercq, A. V. Taichenachev, V. I. Yudin and E. Arimondo, Composite laser-pulses spectroscopy for high-accuracy optical clocks: a review of recent progress and perspectives, *Rep. Prog. Phys.* **81**, 094401 (2018).
- [27] V. I. Yudin, A. V. Taichenachev, M. Y. Basalaev, T. Zanon-Willette, T. Mehlstauber, R. Boudot, J. W. Pollock, M. Shuker, E. A. Donley and J. Kitching, Combined error signal in Ramsey spectroscopy of clock transitions, *New J. Phys.* **20**, 123016 (2018).
- [28] M. Abdel Hafiz, G. Coget, M. Petersen, C. Rocher, T. Zanon-Willette, S. Guérandel, E. de Clercq, and R. Boudot, Toward a high-stability coherent population trapping Cs vapor-cell atomic clock using Autobalanced Ramsey spectroscopy, *Phys. Rev. Appl.* **9**, 064002 (2018).
- [29] M. Abdel Hafiz, G. Coget, M. Petersen, C. E. Calosso, S. Guérandel, E. de Clercq and R. Boudot, Symmetric autobalanced Ramsey interrogation for high-performance coherent population- trapping vapor-cell atomic clock, *Appl. Phys. Lett.* **112**, 244102 (2018).
- [30] M. Shuker, J. W. Pollock, R. Boudot, V. I. Yudin, A. V. Taichenachev, J. Kitching and E. A. Donley, Ramsey spectroscopy with displaced frequency jumps, *Phys. Rev. Lett.* **122**, 113601 (2019).
- [31] M. Shuker, J. W. Pollock, R. Boudot, V. I. Yudin, A. V. Taichenachev, J. Kitching and E. A. Donley, Reduction of light shifts in Ramsey spectroscopy with a combined error signal, *Appl. Phys. Lett.* **114**, 141106 (2019).
- [32] C. Calosso, M. Gozzelino, H. Lin, F. Levi, A. Godone, S. Micalizio, Novel Techniques for Locking the Laser Frequency to the Clock Cell in Vapor Cell Standards, *Proc. 2019 Intern. Freq. Contr. Symp., Paper WeBT2.1*, Orlando, USA (2019).
- [33] S. Jackson and A. C. Vutha, Magic polarization for cancellation of light shifts in two-photon optical clocks, *Phys. Rev. A* **99**, 063422 (2019).
- [34] A. P. Hilton, C. Perella, A. N. Luiten and P. S. Light, Dual-color magic-wavelength trap for suppression of light shifts in atoms, *Phys. Rev. Appl.* **11**, 024065 (2019).
- [35] B. H. McGuyer, Y. Y. Jau and W. Happer, Simple method of light-shift suppression in optical pumping systems, *Appl. Phys. Lett.* **94**, 251110 (2009).
- [36] M. Zhu and L. S. Cutler, U.S. Patent 6,201,821 (2001).
- [37] V. Shah, V. Gerginov, P. D. D. Schwindt, S. Knappe, L. Hollberg, and J. Kitching, Continuous light-shift correction in modulated coherent population trapping clocks, *Appl. Phys. Lett.* **89**, 151124 (2006).
- [38] Y. Zhang, W. Yang, S. Zhang and J. Zhao, Rubidium chip-scale atomic clock with improved long-term stability through light intensity optimization and compensation for laser frequency detuning, *J. Opt. Soc. Am. B* **33**, 8, 1756 (2016).
- [39] D. Miletic, C. Affolderbach, M. Hasegawa, R. Boudot, C. Gorecki and G. Miletì, AC Stark-shift in CPT-based Cs miniature atomic clocks, *Appl. Phys. B* **109**, 89 (2012).
- [40] S. Yanagimachi, K. Harasaka, R. Suzuki, M. Suzuki and S. Goka, Reducing frequency drift caused by light shift in coherent population trapping-based low-power atomic clocks, *Appl. Phys. Lett.* **116**, 104102 (2020).
- [41] V. I. Yudin, M. Yu. Basalaev, A. V. Taichenachev, J. W. Pollock, Z. L. Newman, M. Shuker, A. Hansen, M. T. Hummon, E. A. Donley, and J. Kitching, Universal methods for suppressing the light shift in atomic clocks based on continuous-wave spectroscopy, *ArXiv 1911.02935v1* (2019).
- [42] R. Boudot, V. Maurice, C. Gorecki and E. de Clercq, Pulsed coherent population trapping spectroscopy in microfabricated Cs-Ne vapor cells, *J. Opt. Soc. Am. B* **35**, 5, 1004-1010 (2018).
- [43] C. Thomas, P. Wolf and P. Tavella, Time scales, <https://www.bipm.org/utlis/common/pdf/monographies-misc/Monographie1994-1.pdf> (2020).
- [44] C. E. Calosso, M. Gozzelino, A. Godone, H. Lin, F. Levi and S. Micalizio, Intensity detection noise in pulsed vapor-cell frequency standards, *IEEE Trans. Ultrason. Ferroelec. Freq. Contr.* **67**, 5, 1074-1079 (2020).
- [45] E. Kroemer, J. Rutkowski, V. Maurice, R. Vicarini, M. Abdel Hafiz, C. Gorecki and R. Boudot, Characterization of commercially vertical-cavity surface-emitting lasers tuned on Cs D₁ line at 894.6 nm for atomic clocks, *Appl. Opt.* **55**, 31, 8839-8847 (2016).
- [46] M. Hasegawa, R. K. Chutani, C. Gorecki, R. Boudot, P. Dziuban, V. Giordano, S. Clatot, and L. Mauri, Microfabrication of cesium vapor cells with buffer gas for MEMS atomic clocks, *Sens. Actuators A* **167**, 594-601 (2011).
- [47] O. Kozlova, S. Guérandel and E. de Clercq, Temperature and pressure shift of the Cs clock transition in the

- presence of buffer gases: Ne, N₂, Ar, Phys. Rev. A **83**, 062714 (2011).
- [48] D. Miletic, P. Dziuban, R. Boudot, M. Hasegawa, R. K. Chutani, G. Mileti, V. Giordano and C. Gorecki, Quadratic dependence on temperature of Cs 0-0 hyperfine resonance frequency in single Ne buffer gas microfabricated vapour cell, Elec. Lett. **46**, 15, 1069-1071 (2010).
- [49] O. Kozlova, R. Boudot, S. Guérandel and E. de Clercq, Temperature dependence cancellation of the Cs clock frequency in the presence of Ne buffer gas, IEEE Trans. Instr. Meas. **60**, 7, 2262-2266 (2011).